PHYSICAL REVIEW D **85,** 063503 (2012)

Symmetric and asymmetric light dark matter

Tongyan Lin,[1,*] Hai-Bo Yu,[2,†] and Kathryn M. Zurek[2,‡]

[1]*Physics Department, Harvard University, Cambridge, Massachusetts 02138, USA*

[2]*Michigan Center for Theoretical Physics, Department of Physics, University of Michigan, Ann Arbor, Michigan 48109, USA*

(Received 26 November 2011; published 5 March 2012)

We examine cosmological, astrophysical and collider constraints on thermal dark matter (DM) with mass m_X in the range $\sim$1 MeV–10 GeV. Cosmic microwave background (CMB) observations, which severely constrain light symmetric DM, can be evaded if the DM relic density is sufficiently asymmetric. Cosmic microwave background constraints require the present anti-DM-to-DM ratio to be less than $\sim 2 \times 10^{-6}$ (10^{-1}) for DM mass $m_X = 1$ MeV (10 GeV) with ionizing efficiency factor $f \sim 1$. We determine the minimum annihilation cross section for achieving these asymmetries subject to the relic density constraint; these cross sections are larger than the usual thermal annihilation cross section. On account of collider constraints, such annihilation cross sections can only be obtained by invoking light mediators. These light mediators can give rise to significant DM self-interactions, and we derive a lower bound on the mediator mass from elliptical DM halo shape constraints. We find that halo shapes require a mediator with mass $m_\phi \gtrsim 4 \times 10^{-2}$ MeV (40 MeV) for $m_X = 1$ MeV (10 GeV). We map all of these constraints to the parameter space of DM-electron and DM-nucleon scattering cross sections for direct detection. For DM-electron scattering, a significant fraction of the parameter space is already ruled out by beam-dump and supernova cooling constraints.

DOI: 10.1103/PhysRevD.85.063503 PACS numbers: 95.35.+d

I. INTRODUCTION

Studies of dark matter (DM) have historically focused on particles with weak scale mass $\sim$100 GeV [1–3]. The reason is not only the focus of the high-energy physics community on weak-scale phenomena, but also because the annihilation cross section for a weakly interacting massive particle (WIMP) naturally gives rise to the observed cold DM relic abundance. This is the so-called "WIMP miracle."

More recently, there has been a broader interest in light DM, with mass $m_X \lesssim 10$ GeV. Part of the reason for this interest is phenomenological. Direct detection results from DAMA [4], CoGeNT [5,6], and CRESST [7] claim event excesses that can be interpreted as nuclear scattering of DM with mass $\sim$10 GeV (although the mutual consistency of these results is disputed). Meanwhile, dark matter with masses of MeV has been studied as a possible explanation of the INTEGRAL/SPI 511 keV signal [8–14].

There is also a theoretical motivation for light DM, as DM with mass $m_X \lesssim 10$ GeV appears in certain classes of models naturally. In supersymmetric hidden sector models, for example, gauge interactions generate light DM masses and give rise to the correct annihilation cross section [12,15,16]. The asymmetric DM (ADM) scenario, where the DM particle X carries a chemical potential, analogous to the baryons, provides another approach to light DM (see, e.g., Refs. [17–20] and references therein). In these scenarios, both DM (X) and anti-DM ($\bar{X}$) particles may populate the thermal bath in the early Universe; however, the present number density is determined not only by the annihilation cross section, but also by the DM-number asymmetry η_X. Depending on the value for η_X, the DM mass can be as low as $\sim$keV in ADM models [21], though the natural scale for ADM is set by $(\Omega_{\rm CDM}/\Omega_b)m_p \approx$ 5 GeV.

The purpose of this paper is to explore model-independent constraints and predictions for the asymmetric and symmetric limits of light DM with mass $\sim$1 MeV–10 GeV.[1] Although both phenomenological and theoretical considerations have motivated the study of light DM candidates, there are still a number of important constraints that should be taken into account in realistic model building. In general, light thermal DM faces two challenges: one is to evade bounds on energy injection around redshifts $z \sim$ 100–1000 coming from observations of the cosmic microwave background (CMB); the other is to achieve the required annihilation cross section without conflicting with collider physics constraints.

CMB data from WMAP7 strongly limits DM annihilation during the epoch of recombination and excludes symmetric thermal light DM with mass below $\sim$1–10 GeV if the annihilation is through s-wave processes [22–24]. The CMB bounds may be evaded in the symmetric case if DM

*tongyan@physics.harvard.edu
†haiboyu@umich.edu
‡kzurek@umich.edu

[1]For DM much lighter than $\sim$1 MeV, DM can only annihilate to neutrinos, new light states that remain relativistic through matter-radiation equality, or hidden sector forces that decay invisibly. In this case, the cosmic microwave background and collider bounds discussed here do not apply.

dominantly annihilates to neutrinos or if its annihilation is p-wave suppressed. When the DM relic density is asymmetric, DM annihilation during recombination can be highly suppressed if the symmetric component is sufficiently depleted, providing a natural way to resolve the tension from CMB constraints for light DM scenarios. Unlike the case of symmetric DM, the CMB places a *lower* bound on the annihilation cross section for ADM from the requirement of sufficient depletion of the symmetric component. We calculate the minimum annihilation cross section required in order to evade the CMB bound and achieve the correct relic density simultaneously.

However, it is difficult to achieve the needed annihilation rate to standard model (SM) particles through a weak-scale mediator. Null results from monojet plus missing energy searches at the Tevatron [25–27] and the LHC [28,29] strongly constrain such a mediator if DM couples to quarks and gluons. Meanwhile, the monophoton plus missing energy search at LEP sets limits on the coupling between DM and charged leptons [30] via such a heavy state. These collider constraints are so strong that the annihilation through an off-shell heavy mediator is generally insufficient for ADM to achieve the correct relic density and evade the CMB constraint, if the DM mass is below a few GeV. One way to evade the collider constraints is to invoke a light mediator with mass much less than $\sim$100 GeV. In this case, DM can annihilate to SM states efficiently via the light state without conflicting with collider bounds. Furthermore, if the mediator is lighter than the DM, a new annihilation channel opens, and DM can annihilate dominantly to the mediator directly. In this limit, the mediator particle may couple to the SM sector rather weakly.

The presence of the light mediator has various implications for DM dynamics in galaxies and for cosmology. The light mediator may give rise to significant DM self-interactions (i.e., DM-DM scattering); this is true in both the symmetric and asymmetric limits, since the light state mediates DM-DM interactions as well as anti-DM and DM interactions. These interactions leave footprints in the DM halo dynamics. There are limits on the DM self-interaction cross section coming from observations of elliptical DM halos and elliptical galaxy clusters. We combine these with the relic density constraint to place a lower bound on the mediator mass $\sim 4 \times 10^{-2}$ MeV $-$ 40 MeV for DM masses in the range $\sim$1 MeV–10 GeV. We assume this massive mediator decays to SM relativistic degrees of freedom in the early Universe to avoid the overclosure problem and derive conditions for thermalization of the DM and SM sectors.

These astrophysical and cosmological constraints can be applied to the parameter space of scattering rates in direct detection experiments. We consider DM-nucleon scattering for DM masses of 1–10 GeV and DM-electron scattering for DM masses 1 MeV–1 GeV. In the case of electron scattering, we combine the astrophysical and cosmological constraints with bounds from beam-dump experiments and supernova cooling, which exclude a large region of the allowed parameter space. In addition, the predictions are very different dependent on whether the mediator is heavier or lighter than the DM.

The rest of the paper is organized as follows. In Sec. II, we present the relic density calculation for DM in the presence of a chemical potential. In Sec. III, we study the CMB constraint on ADM models and derive the annihilation cross section required to evade the CMB bound. In Sec. IV, we examine current collider physics constraints on the DM annihilation cross section. In Sec. V, we study the elliptical halo shape constraint on the mediator mass. In Sec. VI, we map out the parameter space for DM direct detection. We conclude in Sec. VII.

II. RELIC DENSITY FOR SYMMETRIC AND ASYMMETRIC DARK MATTER

Our starting point is to establish that the correct relic density of $\Omega_{\rm CDM}h^2 = 0.1109 \pm 0.0056$ [31] can be obtained, where we assume that the annihilation cross section $\langle \sigma v \rangle$ and the asymmetry η_X are floating parameters.

In the usual thermal WIMP scenario, the correct relic density is determined by DM annihilation until freeze-out. For Dirac DM in the symmetric limit, the cold DM relic density is $\Omega_{\rm CDM}h^2 \sim 0.11(6 \times 10^{-26}\ {\rm cm}^3/{\rm s})/\langle \sigma v \rangle$. DM may also carry a chemical potential which leads to an asymmetry between the number density of DM and anti-DM. In this case, when the DM sector is thermalized, the present relic density is determined both by the annihilation cross section and the primordial DM asymmetry $\eta_X \equiv (n_X - n_{\bar{X}})/s$, where n_X, $n_{\bar{X}}$ are the DM and anti-DM-number densities and s is the entropy density. In the asymmetric limit, neglecting any washout or dilution effects, the correct relic density is obtained for a primordial asymmetry given by

$$\eta_X \approx \frac{\Omega_{\rm CDM}}{m_X}\frac{\rho_c}{s_0}, \tag{1}$$

where $s_0 \approx 2969.5\,{\rm cm}^{-3}$ and $\rho_c \approx 1.0540h^2 \times 10^4\,{\rm eV/cm}^3$ are the entropy density and critical density today. In the asymmetric limit, the annihilation cross section is sufficiently large that the thermally-populated symmetric component is a subdominant component of the energy density today.

Depending on the strength of indirect constraints on DM annihilation, light DM scenarios must interpolate between the symmetric and asymmetric limits. We thus require precise calculations of the present anti-DM-to-DM ratio $r_\infty = \Omega_{\bar{X}}/\Omega_X$, which controls the size of indirect signals from DM annihilation. Note that r_∞ is related to the absolute relic densities by

$$\Omega_X = \frac{1}{1-r_\infty}\frac{\eta_X m_X s_0}{\rho_c}, \qquad \Omega_{\bar{X}} = \frac{r_\infty}{1-r_\infty}\frac{\eta_X m_X s_0}{\rho_c}, \tag{2}$$

and the total CDM relic density is $\Omega_{\rm CDM} = \Omega_X + \Omega_{\bar{X}}$.

To compute r_∞, we solve the Boltzmann equations for n_X, $n_{\bar{X}}$ freeze-out in the presence of a nonzero chemical potential [32]. In this work, we focus on the case where DM is in thermal equilibrium with the photon thermal bath through freeze-out. In general, this assumption may not hold if there is a weakly coupled light mediator coupling DM to the SM. We leave the more general case for future work [33], noting that the effects on the relic density are up to $\mathcal{O}(10)$, depending on m_X.

The coupled Boltzmann equations for the species $n_+ = n_X$ and $n_- = n_{\bar{X}}$ are

$$\frac{dn_\pm}{dt} = -3Hn_\pm - \langle\sigma v\rangle[n_+ n_- - n_+^{\rm eq} n_-^{\rm eq}], \tag{3}$$

where $\langle\sigma v\rangle$ is the thermally-averaged annihilation cross section over the X and $\bar{X}$ phase space distributions [34]. The Hubble expansion rate is $H \approx 1.66\sqrt{g_{\rm eff}}T^2/M_{\rm pl}$, where $M_{\rm pl} \approx 1.22 \times 10^{19}$ GeV is the Planck mass and $g_{\rm eff}$ is the effective number of degrees of freedom for the energy density. If there is a primordial asymmetry in X number, then there is a nonzero chemical potential μ which appears in the equilibrium distributions as $n_\pm^{\rm eq} = e^{\pm\mu/T} n^{\rm eq}$. Here, $n_{\rm eq}$ is the usual equilibrium distribution with $\mu = 0$, and, thus, $n_+^{\rm eq} n_-^{\rm eq} = (n^{\rm eq})^2$.

We then take the standard definitions $x = m_X/T$ and $Y_\pm = n_\pm/s$, where $s = (2\pi^2/45)h_{\rm eff}(T)T^3$ is the entropy density and $h_{\rm eff}(T)$ is the effective number of degrees of freedom for the entropy density. We write the annihilation cross section as $\langle\sigma v\rangle = \sigma_0 x^{-n}$, with $n = 0$ and $n = 1$ for s-wave and p-wave annihilation processes, respectively. Then, simplifying Eq. (3) gives

$$\frac{dY_\pm}{dx} = -\frac{\lambda}{x^{n+2}}\sqrt{g_*}(Y_+ Y_- - (Y^{\rm eq})^2), \tag{4}$$

where $\lambda \equiv 0.264 M_{\rm pl} m_X \sigma_0$ and $Y^{\rm eq} \simeq 0.145(g/h_{\rm eff}) \times x^{3/2}e^{-x} \equiv a x^{3/2} e^{-x}$. The effective number of degrees of freedom is $\sqrt{g_*} = \frac{h_{\rm eff}}{\sqrt{g_{\rm eff}}}(1 + \frac{T}{3h_{\rm eff}}\frac{dh_{\rm eff}(T)}{dT})$ [34].

After being generated at some high temperature, the DM asymmetry is a conserved quantity, so we have the constraint

$$\eta_X = Y_+ - Y_-, \tag{5}$$

which is constant at any given epoch.[2] In order to impose this condition on our numerical solutions, we define the departure from equilibrium Δ by $Y_\pm = Y_\pm^{\rm eq} + \Delta$ and instead solve the (single) equation for Δ.

It is helpful to present approximate analytic solutions in the limit of constant $\sqrt{g_*}$ [32,38,39]. Equation (4) can be solved analytically at late times when $(Y^{\rm eq})^2$ becomes negligible. In this limit, using Eq. (5), we can integrate Eq. (4) separately for $\bar{X}$ and X to obtain

$$Y_\pm(\infty) \simeq \frac{\pm\eta_X}{1 - [1 \mp \eta_X/Y_\pm(x_f)]e^{\mp\eta_X\lambda\sqrt{g_*}x_f^{-n-1}/(n+1)}}. \tag{6}$$

These solutions also apply for the symmetric case in the limit of $\eta_X \to 0$. We take the freeze-out temperature $x_f = m_X/T_f$ as derived in Ref. [38]:

$$x_f \simeq \ln[(n+1)\sqrt{g_*}a\lambda] + \frac{1}{2} \times \ln\frac{\ln^2[(n+1)\sqrt{g_*}a\lambda]}{\ln^{2n+4}[(n+1)\sqrt{g_*}a\lambda] - (\sqrt{g_*})^2[(n+1)\lambda\eta_X/2]^2}. \tag{7}$$

Using $Y_\pm(\infty)$ given in Eq. (6), we can obtain the present ratio of the $\bar{X}$ to X number densities:

$$r_\infty \equiv \frac{Y_-}{Y_+}(\infty) \simeq \frac{Y_-(x_f)}{Y_+(x_f)}\exp\left(\frac{-\eta_X\lambda\sqrt{g_*}}{x_f^{n+1}(n+1)}\right). \tag{8}$$

While we can obtain a precise analytic result for $r(x_f) = Y_-(x_f)/Y_+(x_f)$, it turns out that the consequence of neglecting the $(Y^{\rm eq})^2$ in the late-time solution can almost exactly be accounted for by simply setting $r(x_f) = 1$. This gives numerically accurate answers over a wide range of η_X and $\langle\sigma v\rangle$ as discussed in Ref. [38]. Note that the solution here only converges when $\eta_X\lambda$ is small enough, $\sqrt{g_*}\eta_X\lambda < 2x_f^{n+2}$.

III. CMB CONSTRAINTS

For both symmetric and asymmetric thermal DM, the DM particles must have a sufficiently large annihilation cross section in order to achieve the correct relic density. This annihilation may have many indirect astrophysical signatures; among these, the most robust prediction (or constraint) is the effect of DM annihilation on the cosmic microwave background [40], since the effect only depends on the average DM energy density. We first summarize recent studies of CMB constraints on DM annihilation and then discuss scenarios which naturally evade these constraints for light DM, focusing on the asymmetric DM scenario.

Energy deposition from DM annihilation distorts the surface of last scattering, which affects the CMB anisotropies and is thus constrained by WMAP7 data. CMB constraints become increasingly severe for smaller DM masses: the energy released in DM annihilations scales as $\sim m_X(n_X)^2 \sim \rho_{\rm CDM}^2/m_X$, where $\rho_{\rm CDM}$ is the average energy density in DM. This implies the effect of DM annihilation on the CMB scales as $\sim\langle\sigma v\rangle/m_X$. Though

[2] We assume there is no Majorana mass term for DM, and, thus, $X - \bar{X}$ oscillation [21,35–37] does not occur. We also assume there is no entropy production in this case, and there are no DM-number violating interactions at these temperatures.

the precise bound depends on the mass and annihilation channels, WMAP7 limits the amount of annihilation during recombination to below the thermal relic annihilation cross section if $m_X \lesssim 1$–10 GeV [22,23,41,42]. Furthermore, Planck data can improve these constraints by up to a factor of 10.

For self-annihilating DM particles such as Majorana fermions or real scalars, the energy deposition rate per volume at redshift z is

$$\frac{dE}{dtdV}(z) = \rho_c^2 \Omega_{\rm CDM}^2 (1+z)^6 f(z) \frac{\langle \sigma v \rangle_{\rm CMB}}{m_X}, \quad (9)$$

where ρ_c is the critical density at the present time, $\langle \sigma v \rangle_{\rm CMB}$ is the thermally-averaged annihilation cross section at the epoch of recombination, and $f(z)$ parametrizes the amount of energy absorbed by the photon-baryon fluid at redshift z, relative to the total energy released by DM annihilation at that redshift.

The quantity $f(z)$ gives the efficiency of energy deposition at redshift z and thus depends on the spectrum of photons, neutrinos, and $e^{\pm}$ resulting from DM annihilation. In general, the dependence of $f(z)$ on z is mild [41], and an excellent approximation is to take $f(z) \equiv f e_{\rm WIMP}(z)$ where f is a constant and $e_{\rm WIMP}(z)$ is a universal function for WIMP DM [24]. In addition, to leading order $f \simeq (1 - f_\nu)$ [23], where f_ν is the fraction of energy going to neutrinos per annihilation. For DM annihilation channels to charged lepton or pion final states, $f \approx 0.2$–1; here, annihilation only to $e^{\pm}$ can give $f \sim 1$.

There is also some mild m_X dependence in $f(z)$ (or f), since the spectrum of DM annihilation products depends on m_X. Reference [41] computed detailed efficiency curves $f(z)$ for $m_X > 1$–10 GeV, depending on the channel. However, the observed trend is that efficiency does not depend strongly on mass in the range 1–1000 GeV and, furthermore, *increases* for lower mass.[3] We will extrapolate results to $m_X < 1$ GeV; we expect this is a conservative approach.

The WMAP7 limit on DM energy injection at the 95% C.L. can be written as [22]

$$f \frac{\langle \sigma v \rangle_{\rm CMB}}{m_X} < \frac{2.42 \times 10^{-27}\ {\rm cm}^3/{\rm s}}{\rm GeV}. \quad (10)$$

This bound[4] as given assumes DM particles are self-annihilating, i.e. Majorana fermions or real scalars. For DM candidates that are Dirac fermions or complex scalars, as in ADM scenarios, the energy injection rate is

$$\frac{dE}{dtdV}(z) = 2\rho_c^2 \Omega_{\rm CDM}^2 \frac{r_\infty}{(1+r_\infty)^2} (1+z)^6 f(z) \frac{\langle \sigma v \rangle_{\rm CMB}}{m_X}, \quad (11)$$

where we have used $\rho_X + \rho_{\bar{X}} = \rho_{\rm CDM}$ and $r_\infty = \rho_{\bar{X}}/\rho_X$. Note there is factor of 2 in the energy injection rate relative to the self-annihilating case, accounting for the number of possible annihilations. Comparing Eq. (9) and (11), we can translate the bound given in Eq. (10) to the Dirac fermion or complex scalar case:

$$\frac{2r_\infty}{(1+r_\infty)^2} f \frac{\langle \sigma v \rangle_{\rm CMB}}{m_X} < \frac{2.42 \times 10^{-27}\ {\rm cm}^3/{\rm s}}{\rm GeV}. \quad (12)$$

We show this constraint for various r_∞ values in Fig. 1; the dotted black line gives the thermal relic annihilation cross section in the symmetric case, where we have solved for the relic density numerically and taken $f = 1$.

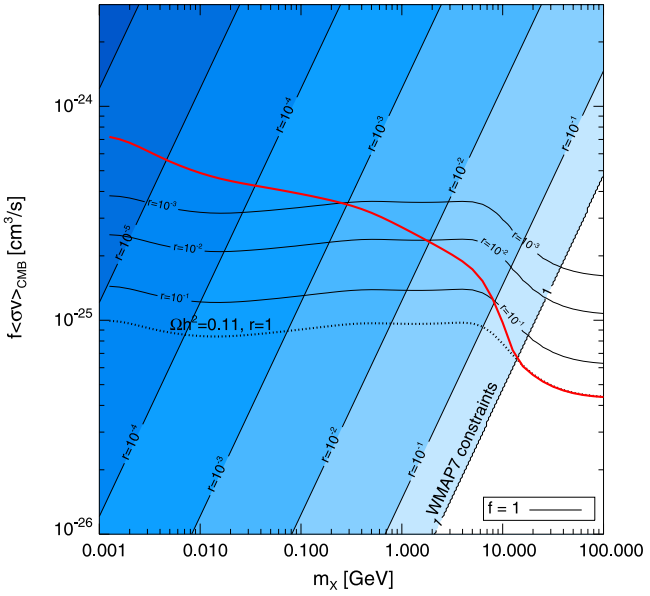

FIG. 1 (color online). WMAP7 95% C.L. constraints on the DM annihilation cross section and mass for asymmetric dark matter and s-wave annihilation. We show constraints for various values of $r = r_\infty = \Omega_{\bar{X}}/\Omega_X$, the anti-DM-to-DM ratio at the present time. The shaded region (blue) is excluded by the WMAP7 data, with different shades corresponding to different r_∞. Along the horizontal contours of constant r are the values of $\langle \sigma v \rangle$, where the correct relic density can be obtained for an efficiency factor $f = 1$. The turnover around $m_X \sim 10$ GeV comes from the drop in SM degrees of freedom when the Universe has temperature ~ 1 GeV. The thick solid (red) line is the intersection of the WMAP7 and relic density contours: it indicates the minimum $\langle \sigma v \rangle$ needed to obtain the observed relic density and satisfy CMB constraints for s-wave annihilation.

[3] Above m_X, $m_\phi > 1$ MeV, most of the annihilation products rapidly cascade down to lower energies, and the efficiency f is only mildly sensitive to the initial energy spectrum of annihilation products (normalizing for the total energy). However, photons in the range $\sim$0.1–1 GeV deposit their energy relatively inefficiently. For annihilation of the sub-GeV scale DM, typically a smaller fraction of the total energy goes into photons of these energies, which increases the total efficiency slightly. We thank Tracy Slatyer for this point.

[4] Note: the results of [23] are slightly weaker by a factor of 1.2–2.

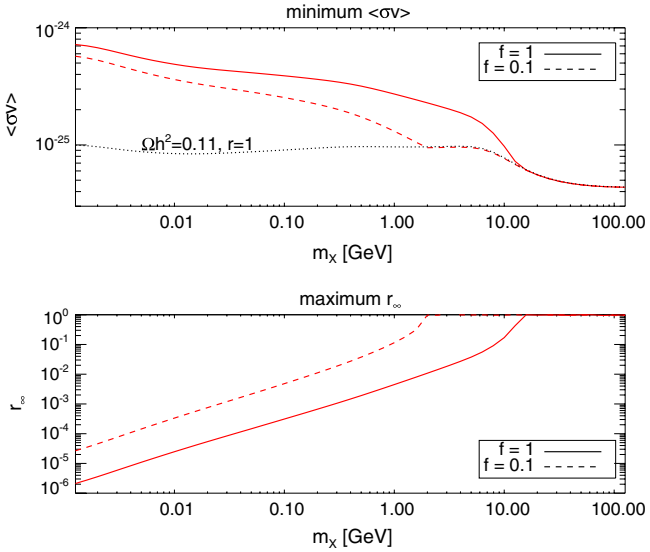

FIG. 2 (color online). (*Top*) Minimum $\langle\sigma v\rangle$ for efficient annihilation of the symmetric component in an ADM scenario, such that CMB bounds can be evaded, for two different values of the efficiency f. The black dotted line gives the thermal relic $\langle\sigma v\rangle$ for the symmetric case. (*Bottom*) The corresponding maximum allowed r_∞, the anti-DM-to-DM ratio at the present time.

ADM can evade CMB bounds while still allowing s-wave annihilation.[5] The CMB bounds do not completely disappear in the ADM scenario, however, because there is a small symmetric component of DM remaining, r_∞, the size of which depends on $\langle\sigma v\rangle$. Because of the exponential dependence of r_∞ on $\langle\sigma v\rangle$, as shown in Eq. (8), the CMB constraints lead to a lower bound on $\langle\sigma v\rangle$. This is shown in Fig. 1, where we map out the constraints in the $\langle\sigma v\rangle_{\rm CMB}$ and m_X parameter space, computing the relic density numerically and applying the constraint in Eq. (10). The solid line (red) gives the resulting lower bound on $f\langle\sigma v\rangle_{\rm CMB}$. This lower bound on $f\langle\sigma v\rangle_{\rm CMB}$ translates to an upper bound on the residual symmetric component, r_∞, as shown in Fig. 2. We give analytic approximations to these numerical solutions next.

When $r_\infty \ll 1$, we can ignore the $\bar{X}$ contribution to the total relic density, and the DM asymmetry parameter η_X is set by $\eta_X \approx \Omega_{\rm CDM}\rho_c/(m_X s_0)$. For a given η_X, the required annihilation cross section at freeze-out to achieve a particular residual symmetric component, r_∞, can be obtained by rewriting Eq. (8) as

$$\langle\sigma v\rangle_f \simeq \frac{s_0 x_f}{0.264\Omega_{\rm CDM}\rho_c\sqrt{g_{*,f}}M_{\rm pl}}\ln\left(\frac{1}{r_\infty}\right) \simeq c_f \times 5\times 10^{-26}\ {\rm cm}^3/{\rm s}\times\ln\left(\frac{1}{r_\infty}\right), \quad (13)$$

where $c_f \equiv (\frac{x_f}{20})(\frac{4}{\sqrt{g_{*,f}}})$ is an $\mathcal{O}(1)$ factor. We show the numerical result as the horizontal contours of constant r_∞ in Fig. 1; for $m_X < 1$ GeV, we obtain a good approximation to the numerical solution by taking $c_f = 1$. On the other hand, the CMB bound on the annihilation cross section when $r_\infty \ll 1$ is

$$\langle\sigma v\rangle_{\rm CMB} < \frac{2.42\times 10^{-27}\ {\rm cm}^3/{\rm s}}{2f}\left(\frac{m_X}{1\ {\rm GeV}}\right)\left(\frac{1}{r_\infty}\right). \quad (14)$$

For s-wave annihilation, we take $\langle\sigma v\rangle_f \simeq \langle\sigma v\rangle_{\rm CMB}$. Since $\langle\sigma v\rangle_f$ increases with $\log(1/r_\infty)$, but the CMB bound on $\langle\sigma v\rangle_{\rm CMB}$ increases with $1/r_\infty$, we can evade the CMB constraints by decreasing r_∞. For a given DM mass, thermal ADM is consistent with the CMB constraints if r_∞ satisfies the following condition:

$$r_\infty\ln\left(\frac{1}{r_\infty}\right) < \frac{2.42\times 10^{-2}}{f\times c_f}\left(\frac{m_X}{1\ {\rm GeV}}\right). \quad (15)$$

The numerical result for this bound is shown in Fig. 2; a good analytic approximation is given by $r_\infty < r_0/\ln(1/r_0)$, with $r_0 \simeq 2\times 10^{-2}(m_X/{\rm GeV})/f$. Taking $f\sim 1$, we can see that r_∞ has to be smaller than 5×10^{-3} and 2×10^{-6} for $m_X \sim 1$ GeV and 1 MeV, respectively.

Likewise, we can combine Eq. (13) and (14) to place a lower bound on $\langle\sigma v\rangle_f$:

$$\frac{\langle\sigma v\rangle_f}{c_f\times 5\times 10^{-26}\ {\rm cm}^3/{\rm s}} \gtrsim \begin{cases} \ln\left(40c_f f\times\frac{1\ {\rm GeV}}{m_X}\right)+\ln\ln\left(40c_f f\times\frac{1\ {\rm GeV}}{m_X}\right), & m_X \lesssim f\times 10\ {\rm GeV}. \\ 2, & m_X \gtrsim f\times 10\ {\rm GeV}. \end{cases} \quad (16)$$

Note if m_X is larger than $f\times 10$ GeV, the CMB constraints do not apply, and the annihilation cross section is set by the relic density requirement. The analytic approximation in Eq. (16) agrees well with the numerical results, which are shown in Fig. 2.

With these constraints on the minimum annihilation cross section, we now turn to discussing what classes of models can generate the needed annihilation cross section consistent with collider constraints.

[5]In the symmetric limit, one can evade the CMB bounds if DM annihilates via p-wave suppressed interactions. Then $\langle\sigma v\rangle_{\rm CMB} \simeq (v_{\rm CMB}/v_f)^2\langle\sigma v\rangle_f$ and since $v_{\rm CMB}\sim 10^{-8}$ while $v_f \sim 0.3$, the annihilation cross section at recombination is highly suppressed, and WMAP constraints are substantially weakened. An increased branching ratio to neutrinos (smaller f) can also alleviate the tension with CMB data for light DM.

IV. LIGHT MEDIATORS

Thus far, we have treated the annihilation cross section $\langle\sigma v\rangle$ as a free parameter. To proceed, we must specify the physics that generates this cross section. First, DM may annihilate directly to SM particles through heavy mediators with mass greater than the weak scale. This coupling to the SM implies light DM can be produced in abundance in colliders. We review constraints from missing (transverse) energy searches at collider experiments and from direct-detection experiments, which conflict with the $\langle\sigma v\rangle$ required to obtain the observed relic density. In this case, thermal light DM is ruled out in both the symmetric and asymmetric scenarios. Second, DM can annihilate via new light states which have a mass below the typical momentum transfer scale in the colliders. In this case, the collider constraint can be evaded. If the new state is lighter than DM, it can be very weakly coupled to the SM.

A. Collider and direct-detection constraints on light DM with heavy mediators

In the heavy mediator case, a convenient way to parametrize the DM-SM coupling is via higher dimensional operators, which is valid if the mediator mass is heavier than the relevant energy scale. Here, we give two typical examples,

$$\mathcal{O}_1: \frac{\bar{X}\gamma_\mu X\bar{f}\gamma^\mu f}{\Lambda_1^2} \quad \text{and} \quad \mathcal{O}_2: \frac{\bar{X}X\bar{f}f}{\Lambda_2^2}, \tag{17}$$

where X is DM, f is a SM fermion, and $\Lambda_{1,2}$ are cutoff scales for $\mathcal{O}_{1,2}$. The cutoff scale, in terms of the parameters in the UV-complete models, is $\Lambda = m_\phi/\sqrt{g_X g_f}$, where m_ϕ is the mediator mass, and g_X and g_f are coupling constants of DM-mediator and SM-mediator interactions, respectively.

In the limit of $m_X \gg m_f$, the DM annihilation cross sections at freeze-out are given by

$$\langle\sigma v\rangle_1 \simeq \frac{N_f^c}{\pi}\frac{m_X^2}{\Lambda_1^4} \quad \text{and} \quad \langle\sigma v\rangle_2 \simeq \frac{N_f^c}{8\pi}\frac{m_X^2}{\Lambda_2^4}\frac{1}{x_f}, \tag{18}$$

for $\mathcal{O}_1$ and $\mathcal{O}_2$, respectively. N_f^c is the color multiplicity factor of fermion f, and $x_f = m_X/T \approx 20$, with T the temperature. Note that the annihilation cross section through $\mathcal{O}_2$ is p-wave suppressed. Now, we can estimate the limit on the cut-off scales Λ_1 and Λ_2 by requiring the correct relic density

$$\Lambda_1 \lesssim 370\ \text{GeV}\left(\frac{N_f^c}{3}\right)^{(1/4)}\left(\frac{m_X}{10\ \text{GeV}}\right)^{(1/2)} \times \left(\frac{6\times 10^{-26}\ \text{cm}^3/\text{s}}{\langle\sigma v\rangle}\right)^{(1/4)}, \tag{19}$$

$$\Lambda_2 \lesssim 100\ \text{GeV}\left(\frac{N_f^c}{3}\right)^{(1/4)}\left(\frac{m_X}{10\ \text{GeV}}\right)^{(1/2)} \times \left(\frac{6\times 10^{-26}\ \text{cm}^3/\text{s}}{\langle\sigma v\rangle}\right)^{(1/4)}\left(\frac{20}{x_f}\right)^{(1/4)}, \tag{20}$$

where the limit is relevant for both the asymmetric and symmetric cases. Since the annihilation cross section is p-wave suppressed for $\mathcal{O}_2$, we need a smaller cut-off scale to obtain the correct relic abundance. Now, we review various constraints on the cut-off scales $\Lambda_{1,2}$:

(i) *Direct Detection Constraints*
If DM couples to quarks, the operators $\mathcal{O}_{1,2}$ can lead to direct-detection signals with the DM-nucleon scattering cross section: $\sigma_{n_{1,2}} \sim \mu_n^2/\Lambda_{1,2}^4$, and μ_n is the DM-nucleon reduced mass. For a DM mass $\sim$10 GeV, taking the value of $\Lambda_{1,2}$ given in Eqs. (19) and (20), we expect the DM-nucleon scattering cross section to be $\sigma_{n_1} \sim 10^{-38}$ cm^2 and $\sigma_{n_2} \sim 10^{-36}$ cm^2. However, the current upper bound on σ_n from direct-detection experiments for DM with mass $m_X \gtrsim 10$ GeV is $\sigma_n \lesssim 10^{-42}$ cm^2 [43], which is much smaller than the predicted values from requiring the correct thermal relic density. For DM with mass below a few GeV, the recoil energies are too small and direct-detection bounds are currently very weak or nonexistent.

(ii) *Tevatron and LHC Constraints*
The DM-quark interactions given in $\mathcal{O}_{1,2}$ can lead to signals of monojet plus missing transverse energy at hadron colliders, while the Tevatron data for this signal matches the SM prediction well. We require that $\mathcal{O}_{1,2}$ do not give rise to sizable contributions to this signal. The lower bounds on $\Lambda_{1,2}$ are $\sim$400 GeV and $\sim$400 GeV [25–27], respectively, for DM masses $m_X \lesssim 10$ GeV that we are interested in. Recent LHC results give a stronger limit on $\Lambda_1 \gtrsim 700$ GeV [29]. Therefore, the Tevatron and LHC searches have excluded both thermal symmetric DM and ADM in the whole range of light DM if the DM particles annihilate to light quarks through $\mathcal{O}_1$ and $\mathcal{O}_2$.

(iii) *LEP Constraints*
If DM particles couple to the electron through $\mathcal{O}_{1,2}$, the monophoton search at LEP sets a limit on the cutoff scale: $\Lambda_1 \gtrsim 480$ GeV and $\Lambda_2 \gtrsim 440$ GeV for DM mass $m_X \lesssim 10$ GeV [30]. Note the limit also applies to the case where DM couples to three generations of charged leptons universally. One may avoid the limit by coupling DM only to μ or τ. However, this approach usually involves model building complications and severe flavor constraints.

Thus, we conclude that for $\mathcal{O}_{1,2}$, DM does not have the correct relic abundance for symmetric DM and

ADM due to the combination of direct detection and collider constraints. The direct detection constraints can be relaxed by suppressing the direct-detection scattering cross section; this can happen, for example, if the scattering of nuclei is velocity-suppressed, notably through an axial interaction. However, the collider bounds are still severe for higher-dimensional operators involving interactions with light quarks or electrons [25–30].

B. Light dark matter with light mediators

One simple way to evade the collider constraints for light DM is to invoke light mediators with masses much smaller than the typical transverse momentum of the colliders $p_T \sim \mathcal{O}(100\ \mathrm{GeV})$ (or the center-of-mass energy $\sim$200 GeV for LEP). In this limit, the effective theory approach breaks down, and the collider bounds become much weaker [27,29,30,44]. In general, if the mediator mass is much less than the p_T probed at colliders, there exists a large parameter space for light-DM scenarios to achieve the correct relic density. We consider a hidden sector with Dirac DM coupled to a light mediator which could be a spin-1 or spin-0 particle; for ease of notation, we always refer to it as ϕ. We write the Lagrangians as

$$\mathcal{L}_V = g_X \bar{X}\gamma^\mu X \phi_\mu + g_f \bar{f}\gamma^\mu f \phi_\mu + m_X \bar{X}X + m_\phi^2 \phi^\mu \phi_\mu, \tag{21}$$

$$\mathcal{L}_S = g_X \bar{X}X\phi + g_f \bar{f}f\phi + m_X \bar{X}X + m_\phi^2 \phi^2, \tag{22}$$

where m_ϕ is the mediator mass. We consider two cases for the mediator mass[6]: a mediator with $m_\phi > 2m_X$ and lighter mediator with $m_\phi < m_X$.

In the case of $p_T \gg m_\phi > 2m_X$, the DM particles can annihilate to SM particles through the s-channel process. There is a collider bound on g_f because an on-shell mediator which decays to $X\bar{X}$ can be produced, potentially contributing to the monojet plus missing transverse energy signal. Tevatron data has been employed to place an upper bound on $g_f < 0.015/\sqrt{Br(\phi \to X\bar{X})}$ for $m_\phi < 20$ GeV [44], where $Br(\phi \to X\bar{X})$ is the branching ratio of ϕ decay to the DM pair. In this case, the annihilation cross section is given by $\langle\sigma v\rangle_V \simeq 4\alpha_X g_f^2 m_X^2 N_f^c / m_\phi^4$ and $\langle\sigma v\rangle_S \simeq \alpha_X g_f^2 m_X^2 N_f^c / 2m_\phi^4 x_f$, where $\alpha_X \equiv g_X^2/4\pi$. To see how the collider constraint affects the annihilation cross section in this case, we take the conservative limit $g_f \lesssim 0.015$, setting $Br(\phi \to X\bar{X}) \sim 1$. From the relic density constraint, we then obtain an upper bound on the mediator mass,

$$m_\phi \lesssim 13\ \mathrm{GeV}\left(\frac{\alpha_X}{10^{-1}}\right)^{1/4}\left(\frac{10^{-25}\ \mathrm{cm}^3/\mathrm{s}}{\langle\sigma v\rangle}\right)^{1/4}\left(\frac{m_X}{1\ \mathrm{GeV}}\right)^{1/2}. \tag{23}$$

This bound[7] is consistent with our assumption that $m_\phi \gg m_X$.

If $m_\phi < m_X$, DM can annihilate to the mediator directly, and the annihilation cross section is determined primarily by the hidden sector coupling g_X:

$$\begin{aligned}\langle\sigma v\rangle_V &= \frac{\pi\alpha_X^2}{m_X^2}\sqrt{1-\left(\frac{m_\phi}{m_X}\right)^2}, \\ \langle\sigma v\rangle_S &= \frac{9}{2}\frac{\pi\alpha_X^2}{m_X^2}\frac{T}{m_X}\sqrt{1-\left(\frac{m_\phi}{m_X}\right)^2},\end{aligned} \tag{24}$$

for the vector and scalar mediators, respectively. Meanwhile, g_f determines how the DM sector couples to the SM sector. As for the collider physics, the production of $X\bar{X}$ occurs through an off-shell mediator; since this is a three-body process, the bound is rather weak. Tevatron data requires $g_f \lesssim 0.2$ if the mediator couples to quarks universally [44].

Although g_f does not appear to play an important role in the relic density, this coupling controls the width (lifetime) of ϕ and is relevant for cosmology. The width Γ_ϕ of the mediator is

$$\begin{aligned}(\Gamma_\phi)_V &= \frac{4N_f^c}{3}\frac{m_\phi}{16\pi}g_f^2\sqrt{1-\left(\frac{2m_f}{m_\phi}\right)^2}, \\ (\Gamma_\phi)_S &= 2N_f^c\frac{m_\phi}{16\pi}g_f^2\sqrt{1-\left(\frac{2m_f}{m_\phi}\right)^2},\end{aligned} \tag{25}$$

where the lifetime $\tau_\phi = \Gamma_\phi^{-1}$. In Sec. II, we assumed the DM particles to be in thermal equilibrium with the SM thermal bath in the early Universe, and in this case, the standard freeze-out picture and cosmology apply. Now, we check the condition for thermalization of the two sectors. If the mediator decay rate is larger than the Hubble expansion rate at temperatures $T > m_\phi$, then the inverse decay processes can keep ϕ in chemical equilibrium with the SM thermal bath [45]. At these temperatures, the decay rate is given by $\Gamma_\phi \sim g_f^2 m_\phi^2/(16\pi T)$, where the factor of m_ϕ/T accounts for the effect of time dilation. In order for the mediator to stay in thermal equilibrium with the SM thermal bath through DM freeze-out, we require $\Gamma_\phi \gtrsim H$ at temperatures $T \sim m_X$. This gives a constraint on g_f:

[6]In this paper, we do not consider the intermediate case $m_\phi \sim 2m_X$, where there is a resonance in the s-channel annihilation of $\bar{X}X$.

[7]Note that in this case, there are also strong bounds on m_ϕ from neutrino experiments [13]; however, we have checked that it is still possible to obtain the correct relic density and that the direct-detection predictions are unaffected.

$$g_f \sim \sqrt{\frac{16\pi\Gamma_\phi}{m_\phi}} \gg 8\times 10^{-8}\left(\frac{\sqrt{g_{\rm eff}}}{9}\right)^{1/2}\left(\frac{m_X}{\rm GeV}\right)^{3/2} \times\left(\frac{100\ {\rm MeV}}{m_\phi}\right). \quad (26)$$

If g_f is less than the bound given in Eq. (26), the DM sector can have a different temperature from the SM sector, and the standard freeze-out calculation can be modified in a number of ways. We have checked that these effects lead to change in the minimum annihilation cross section by less than a factor $\mathcal{O}(10)$, compared to the results we derived in Sec. II and III. Furthermore, the massive mediator is a late-decaying particle and, in the case where the mediator decays to the SM states, can modify standard nucleosynthesis (BBN). There are stringent constraints on the hadronic decay of long-lived particles from the ^{4}He fraction, which requires that the lifetime of the mediator be less than 10^{-2} s [46–48]. This leads to a lower bound of $g_q \gtrsim 1.6\times 10^{-11}\sqrt{1\ {\rm GeV}/m_\phi}$ for a vector mediator, where we take $N_f^c = 3$. For leptonic decay modes, we take the lifetime of the mediator $\tau_\phi \lesssim 1s$, and obtain a slightly weaker bound, $g_e \gtrsim 5\times 10^{-11}\sqrt{10\ {\rm MeV}/m_\phi}$, for a vector mediator with $N_f^c = 1$.

Finally, we comment on the calculation of the relic density and application of the CMB constraints in the light mediator case. When $m_\phi < m_X$, $\bar{X}X$ can annihilate to $\phi\phi$, but ϕ decays to standard-model particles rapidly compared to the relevant time scales at recombination so that the CMB constraints are unchanged. The only difference between a heavy mediator and light mediator with large width is whether there is a contribution to the effective degrees of freedom, g_*, from the light mediator. A slightly higher g_* in the light mediator case gives rise to smaller r_∞, which in turn weakens the lower bound on $\langle\sigma v\rangle$ from CMB constraints.

In addition, we have neglected the Sommerfeld enhancement effect. As we will discuss in the following section, the mediator mass is bounded from below by DM halo shapes; this limits the size of any Sommerfeld enhancement. In addition, since $\langle\sigma v\rangle \approx \pi\alpha_X^2/m_X^2$, for light DM the coupling α_X can be much smaller and still satisfy the relic density constraint. For the DM masses considered here, we have checked that the Sommerfeld enhancement effect is negligible for s-wave and p-wave annihilation processes at both freeze-out and during recombination, if we take α_X and m_ϕ close to their minimum allowed values.

V. HALO SHAPE CONSTRAINTS ON THE MEDIATOR MASS

The presence of the light mediator allows for significant DM self-interactions, which can have nontrivial effects on DM halo dynamics. A number of astrophysical observations constrain DM self-interactions, for example, observations of the Bullet Cluster [49], elliptical galaxy clusters [50], and elliptical DM halos [51,52]. Among these, the upper bound on DM self-interaction from the ellipticity of DM halos is the strongest [51]. DM self-interactions can erase the velocity anisotropy and lead to spherical DM halos, so the observed ellipticity of DM halos constrains the DM self-scattering rate. Because the strength of self-interaction increases as the mediator mass decreases, we can use the elliptical halo shape constraint to place a lower limit on the mediator mass. Note that in the case of $m_\phi = 0$, the ellipticity of the DM halos then places a strong upper limit on the hidden sector coupling g_X [53]; it is only possible to obtain the correct relic density if $m_X \gtrsim 10^3$ GeV [51,54].[8]

The effect of DM self-interactions on DM halo shapes can be parametrized by the average rate for DM particles to change velocities by $\mathcal{O}(1)$ [52]:

$$\Gamma_k = \int d^3v_1 d^3v_2 f(v_1) f(v_2)(n_X v_{\rm rel}\sigma_T)(v_{\rm rel}^2/v_0^2), \quad (27)$$

where n_X is the DM density in the DM halo, $v_{\rm rel} = |\vec{v}_1 - \vec{v}_2|$, and $f(v)$ is the DM velocity distribution in the DM halo, for which we take $f(v) = e^{-v^2/v_0^2}/(v_0\sqrt{\pi})^3$. σ_T is the scattering cross section weighted by the momentum transfer: $\sigma_T = \int d\Omega_*(d\sigma/d\Omega_*)(1-\cos\theta_*)$.

The form of σ_T depends on the particle physics nature of DM self-interactions and the relevant momentum scales. If the mediator is lighter than the typical momentum transfer in collisions, DM particles interact through long-range forces, and σ_T depends on velocity. In the opposite limit where the mediator is heavy compared to momentum transfer, DM self-interactions are contact interactions, and σ_T is independent of $v_{\rm rel}$. In this case, we can take the σ_T out of the velocity integrals in Eq. (27) and the calculation is straightforward. We first will derive the upper bound on the DM self-interaction cross section assuming a contact interaction and then show that this limit applies in deriving the minimum mediator mass.

We consider the well-studied elliptical galaxy NGC720 [56,57], taking our bound from the observed ellipticity at a radius of 5 kpc. The DM density profile is fit with local density 4 GeV/cm^3 and radial velocity dispersion $\bar{v}_r^2 = v_0^2/2 \simeq (240\ {\rm km/s})^2$. We require the average time for DM self-interactions to create $\mathcal{O}(1)$ changes on DM velocities to be larger than the galaxy lifetime $t_g \sim 10^{10}$ years, i.e. $\Gamma_k^{-1} > t_g$. This gives the upper bound

$$\sigma_T \lesssim 4.4\times 10^{-27}\ {\rm cm}^2\left(\frac{m_X}{1\ {\rm GeV}}\right)\left(\frac{10^{10}\ {\rm years}}{t_g}\right). \quad (28)$$

[8]This limit can be relaxed if the hidden sector is much colder than the visible sector when DM freezes out. In this case, DM can achieve the correct relic density with a smaller annihilation cross section [55].

The reader should bear in mind that this is an analytic estimate, and detailed N-body simulations studying a range of elliptical galaxies are required for a robust bound.

Other astrophysical constraints have been derived for σ/m_X, assuming a hard sphere scattering cross section σ. A similar bound derived from shapes of elliptical galaxy clusters is $(\sigma/m_X \lesssim 10^{-25.5}\ \mathrm{cm}^2(m_X/\mathrm{GeV}))$ [50]. Specifically, this estimate is obtained from the inner regions of the galaxy cluster MS2137-23, at a radius of 70 kpc with dark matter density $\sim 1\ \mathrm{GeV/cm}^3$. Cosmological simulations of cluster-sized objects support this estimate within an order of magnitude [58]; however, the bound is still based on a single cluster. There is also a bound derived from the Bullet Cluster $[\sigma/m_X \lesssim 2 \times 10^{-24}\ \mathrm{cm}^2(m_X/\mathrm{GeV})]$ [49], reproduced in simulations of the collision by Ref. [59]. Note that this result is not derived from the shapes of the merging clusters but from requiring that the subcluster does not lose a significant fraction of its mass in passing through the larger cluster; however, we have found that the bound is too weak in this case to give a minimum mediator mass.

For the vector and scalar interactions considered here, the force is described by a Yukawa potential $V(r) = \pm\alpha_X e^{-m_\phi r}/r$. Depending on the mediator, and whether we are in the asymmetric limit, the sign may be positive or negative. For the vector case, we have both XX interactions (+) and $X\bar{X}$ interactions (−) unless we are in the asymmetric limit. For the scalar case, the sign is always negative. However, in the limit of a contact interaction, the sign of the potential does not matter. The momentum transfer cross section for scattering through t- and u-channel processes in the Born approximation is

$$\sigma_T \approx \frac{4\pi\alpha_X^2 m_X^2}{m_\phi^4}, \tag{29}$$

which is subject to the bound in Eq. (28). We have assumed a contact interaction, $m_X v_{\mathrm{rel}}/m_\phi \ll 1$; we will justify later that this is a valid assumption in deriving the bounds below.

On the other hand, the relic density constraint places a lower bound on the annihilation cross section $\langle\sigma v\rangle \gtrsim 10^{-25}\ \mathrm{cm}^3/\mathrm{s}$ for light DM and thus on α_X:

$$\alpha_X|_V \gtrsim 5 \times 10^{-5}\left(\frac{\langle\sigma v\rangle}{10^{-25}\ \mathrm{cm}^3/\mathrm{s}}\right)^{1/2}\left(\frac{m_X}{\mathrm{GeV}}\right),$$
$$\alpha_X|_S \gtrsim 11 \times 10^{-5}\left(\frac{\langle\sigma v\rangle}{10^{-25}\ \mathrm{cm}^3/\mathrm{s}}\right)^{1/2}\left(\frac{m_X}{\mathrm{GeV}}\right)\left(\frac{x_f}{20}\right)^{1/2}, \tag{30}$$

for vector and scalar coupling, respectively. Note that we assume $m_\phi < m_X$ and take the annihilation cross sections in Eq. (24).

Since α_X cannot be arbitrarily small, m_ϕ cannot be made arbitrarily small. Combining the bound on α_X with Eq. (29), we obtain a lower bound on the mediator mass:

$$m_\phi|_V \gtrsim 7\ \mathrm{MeV}\left(\frac{\langle\sigma v\rangle}{10^{-25}\ \mathrm{cm}^3/\mathrm{s}}\right)^{1/4}\left(\frac{m_X}{\mathrm{GeV}}\right)^{3/4},$$
$$m_\phi|_S \gtrsim 11\ \mathrm{MeV}\left(\frac{\langle\sigma v\rangle}{10^{-25}\ \mathrm{cm}^3/\mathrm{s}}\right)^{1/4}\left(\frac{x_f}{20}\right)^{1/4}\left(\frac{m_X}{\mathrm{GeV}}\right)^{3/4}, \tag{31}$$

for the vector and scalar mediator cases, where we take the elliptical galaxy with $t_g = 10^{10}$ years. Note that because the bound on m_ϕ scales as $\sigma_T^{-1/4}$ in the contact interaction limit, the result is not very sensitive to the precise bound on σ_T.

In deriving the above bound on m_ϕ, we have assumed that $m_\phi \gg m_X v_{\mathrm{rel}}$ and that the Born approximation is valid. Now, we check that the bound given in Eq. (31) is consistent with these assumptions. The condition $m_\phi \gg m_X v_{\mathrm{rel}}$ is satisfied for $1\ \mathrm{MeV} < m_X < 10\ \mathrm{GeV}$, since from Eq. (31), we have $m_\phi/m_X \sim 10^{-2}(m_X/\mathrm{GeV})^{-1/4}$ but $v_{\mathrm{rel}} \sim 10^{-3}$. In this limit, the Born approximation is valid if the following condition is satisfied:

$$m_X \left| \int_0^\infty r V(r) dr \right| = \frac{m_X \alpha_X}{m_\phi} \ll 1. \tag{32}$$

From Eq. (30), we can see $v_{\mathrm{rel}} \gg \alpha_X$ in the DM mass range we are interested in, and thus this condition is also satisfied if $m_\phi \gg m_X v_{\mathrm{rel}}$. We emphasize that we *cannot* extrapolate the lower mass bound given in Eq. (31) to $m_X \gtrsim 50\ \mathrm{GeV}$ because the Born approximation breaks down. For these higher masses, in general, one has to solve the scattering problem numerically [60]. In the classical limit where $m_X v_{\mathrm{rel}} \gg m_\phi$, there is a fitting formula

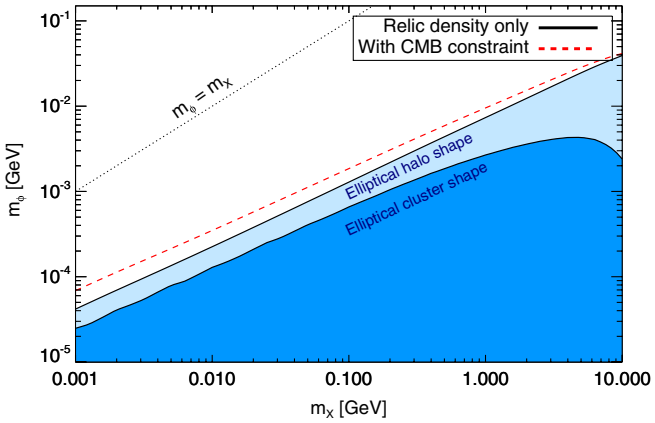

FIG. 3 (color online). Lower limit on the mediator mass from combining relic density and DM self-interaction constraints. We show the case of a vector mediator; the result for a scalar mediator is similar and is given in Eq. (31). We consider DM self-interaction constraints from elliptical halo shapes and elliptical cluster shapes. Bullet cluster constraints do not give a lower bound on m_ϕ. The dashed red line indicates the bound on the mass from elliptical halo shapes if CMB bounds are also applied, assuming efficiency $f \approx 1$.

available in Ref. [61] for the transfer cross section, which has been used to study self-interactions via a light mediator for DM masses greater than ~100 GeV [45,52,62,63].

In Fig. 3, we show the lower limit on m_ϕ for the vector case, including the result derived from the more conservative bounds from elliptical cluster shapes. We also show the slightly stronger result if we take the CMB constraint on the cross section,[9] given in Eq. (17). There is a turnover for the elliptical cluster bounds because the contact interaction limit breaks down; here, we use the full cross section, again in the Born approximation, given in Ref. [52]. The bounds from the Bullet Cluster, which we derive following Ref. [51], do not give rise to a lower bound on m_ϕ.

VI. DIRECT DETECTION

Given the experimental effort needed to detect DM directly, it is important to map out the parameter space of direct-detection cross sections, subject to the astrophysical and cosmological constraints we have discussed. Current experiments are not sensitive to DM-nucleon scattering if the DM mass is below ~1 GeV because of the energy thresholds. It has been suggested that DM-electron scattering may provide an alternative way for the detection of light DM [64]. We consider DM-nucleon scattering for $m_X \gtrsim 1$ GeV and DM-electron scattering for 1 MeV $\lesssim m_X \lesssim 1$ GeV.

We compute the range of allowed elastic scattering cross sections within the framework of light DM annihilating via hidden sector mediators, assuming mediator couplings to electrons or light quarks. We consider both lighter mediators, $m_\phi < m_X$, and heavier mediators, where we focus on the case $m_\phi \gg m_X$. When $m_\phi < m_X$, the mediator can be very weakly coupled to the SM, and so the scattering cross sections can be much smaller than when $m_\phi \gg m_X$. However, there is still a lower limit on the cross section coming from the lower bounds on the couplings of the mediator to the DM and SM fermions, α_X and g_f, respectively. The lower bound on α_X is derived from requiring that relic density and CMB constraints are satisfied. We consider two possible lower bounds on g_f: from requiring the thermalization between the DM and SM sectors, or from requiring decay of the mediator before BBN. When $m_\phi \gg m_X$, the lower limit on the cross section arises purely from the relic density and CMB constraints.

Meanwhile, we obtain upper bounds on the electron scattering cross section from the combination of halo-shape bounds and requiring that the mediator does not significantly affect the electron anomalous magnetic moment. Including supernova and beam-dump constraints on the dark force coupling [65] then carves out a nontrivial part of the parameter space for electron scattering.

[9] In the scalar case, annihilation is p-wave suppressed, and thus CMB constraints do not apply.

Figure 4 summarizes our results for the case where the mediator is a vector. We show the possible DM-nucleon (left panel) and DM-electron (right panel) scattering cross sections as a function of DM mass. The green shaded region is the parameter space for $m_\phi < m_X$ which is allowed by the constraints from the relic density, BBN, and DM halo shape constraints; in the electron case, we include beam-dump and supernova cooling constraints. The lighter green area is set by the additional assumption that the mediator has large decay width and thus that the two sectors are in thermal equilibrium. In the nucleon scattering case, $m_\phi \gg m_X$ is ruled out by CRESST-I and XENON10. In the electron scattering case, the red shaded region labeled $m_\phi \gg m_X$ gives the allowed cross sections. In the following sections, we derive these results and present more details.

A. Nucleon scattering

We first consider nucleon scattering in the mass range 1 GeV $\lesssim m_X \lesssim$ 10 GeV, taking universal couplings to the light quarks given by g_q. The DM-nucleon scattering cross section is given by

$$\sigma_n = 4\alpha_X g_n^2 \frac{\mu_n^2}{m_\phi^4}, \tag{33}$$

where μ_n is the WIMP-nucleon reduced mass, and $g_n = 3g_q$ is the ϕ_μ-nucleon coupling constant. The upper bounds here are set by results from direct-detection experiments, in particular, CRESST-I [66] and XENON10 [67]. We have taken a contact interaction; this is a good approximation over much of the parameter space because the momentum transfer is generally less than the minimum mediator mass allowed by the ellipticity of DM halos, as discussed in Sec. V. We note that momentum dependence can be relevant for scattering off heavier nuclei such as xenon if we take m_ϕ to be close to this minimum value and thus can change the upper limit from XENON10 [68–70]. However, the lower limit is obtained in the limit that $m_\phi \approx m_X$, and thus momentum dependence will not be important. We therefore consider the bounds on a contact interaction for simplicity.

To determine the lower limit on this cross section, we bound α_X and g_q from below in the case that the mediator is lighter than the DM, $m_\phi < m_X$. For thermal DM and masses $m_X > 1$ GeV, a lower bound on α_X is determined primarily by the relic density. As described in Sec. III, CMB constraints are only important in this mass range if ϕ_μ decays dominantly to electrons, for which the efficiency factor is $f \sim 1$. For ϕ_μ coupling primarily to quarks, $f \approx 0.2$ and CMB bounds do not apply above $m_X \sim 2$ GeV. Then the minimum annihilation cross section is $\langle \sigma v \rangle \approx \pi \alpha_X^2 / m_X^2 \approx 10^{-25}$ cm^3/s, giving a bound of $\alpha_X \gtrsim 5.2 \times 10^{-5} (m_X/\text{GeV})$. Requiring thermal equilibrium between the hidden and visible sectors, we take the

bound on g_q in Eq. (26), with $\sqrt{g_{\rm eff}} \approx 9$. Combining the limits above results in a lower bound on the nucleon scattering cross section:

$$\sigma_n \gtrsim 10^{-48}\ \text{cm}^2 \times \left(\frac{m_X}{\text{GeV}}\right)^4 \left(\frac{\text{GeV}}{m_\phi}\right)^6 \left(\frac{\mu_n}{0.5\ \text{GeV}}\right)^2. \quad (34)$$

Since $m_\phi < m_X$, this quantity is saturated for any m_X if we set m_ϕ to its maximum value of $m_\phi \sim m_X$. This bound is indicated by the "large width" line in Fig. 4. Coincidentally, the lower limit here is similar to the best achievable sensitivity for WIMP-nucleon scattering if the dominant irreducible background is a coherent scattering of atmospheric neutrinos off of nuclei [71–73]. However, these studies focused on WIMP DM; for light DM, solar neutrinos become much more important, and the best achievable sensitivity may be several orders of magnitude weaker.

The lower bound on σ_n given in Eq. (34) is derived by requiring the two sectors to be in thermal equilibrium. We may relax this assumption and just demand the mediator decay by nucleosynthesis. This gives $g_q \gtrsim 1.6 \times 10^{-11}\sqrt{1\ \text{GeV}/m_\phi}$, as discussed in Sec. IV B. For such g_q, the two sectors are decoupled through freeze-out; then, the relic density calculation is slightly more complicated and depends on the thermal history of the sectors. The change in the relic density then modifies the bound on α_X. We have checked that the full calculation generally only changes the bound on α_X by an $\mathcal{O}(1)$ factor [33], so here we take the bound on α_X from the large ϕ width case for simplicity. In this limit, the lower bound on σ_n is given by

$$\sigma_n \gtrsim 5 \times 10^{-54}\ \text{cm}^2 \times \left(\frac{m_X}{\text{GeV}}\right)\left(\frac{\text{GeV}}{m_\phi}\right)^5 \left(\frac{\mu_n}{0.5\ \text{GeV}}\right)^2, \quad (35)$$

labeled as "decay before BBN" in Fig. 4.

For reference, we also give the lower bound on the cross section in the case where $m_\phi \gg m_X$. Here, DM annihilation occurs directly to SM final states through ϕ_μ, with annihilation cross section $\langle\sigma v\rangle = 4\alpha_X g_n^2 m_X^2/m_\phi^4$. Since the same combination of parameters enters in both the annihilation cross section and the nucleon scattering cross section, we can directly apply the relic density constraint to obtain

$$\sigma_n \gtrsim 5 \times 10^{-37}\ \text{cm}^2 \left(\frac{1\ \text{GeV}}{m_X}\right)^2 \left(\frac{\mu_n}{0.5\ \text{GeV}}\right)^2. \quad (36)$$

This is the "$m_\phi \gg m_X$" line in Fig. 4. However, this scenario is ruled out by the direct-detection limits on the cross section.

B. Electron scattering

We consider scattering off electrons for DM in the mass range 1 MeV $< m_X <$ 1 GeV. The DM-electron scattering cross section is

$$\sigma_e = 4\alpha_X g_e^2 \frac{\mu_e^2}{m_\phi^4}. \quad (37)$$

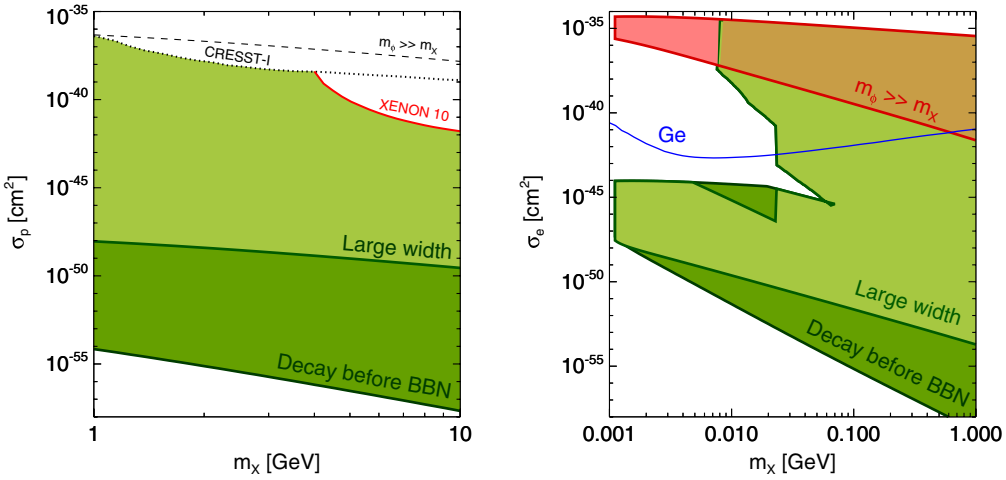

FIG. 4 (color online). *(Left)* Nucleon scattering through a vector mediator. The green shaded region indicates the allowed parameter space of direct-detection cross sections. The lighter green region (labeled "Large width") imposes the bound of thermal coupling between the two sectors while the larger shaded area encompassing this region only requires mediator decay before BBN. Also shown is the lower bound for the heavy mediator ($m_\phi \gg m_X$) case. *(Right)* Electron scattering through a vector mediator, for $m_\phi < m_X$ (green) and $m_\phi \gg m_X$ (red); the intersection of the two regions is shaded brown. We show the projected sensitivity of a Ge experiment, taken from Ref. [64]. Beam-dump, supernova, and halo-shape constraints apply here and carve out the region of large σ_e at low m_X. For more details, see the text. In the lighter green region labeled "Large width," the condition of thermal equilibrium between the visible and hidden sectors is imposed.

The lower bound on the scattering cross section can be derived in the same way as in the nucleon case, taking $m_\phi < m_X$. Here, both CMB and relic density constraints apply, since $m_X < 1$ GeV, and the energy deposition efficiency $f \approx 1$ for decay to electrons. We take the bound on the annihilation cross section in Eq. (16) with $c_f \approx 1$, giving a lower limit on α_X:

$$\alpha_X \gtrsim 4 \times 10^{-7} \left(\frac{m_X}{10\ \text{MeV}}\right) \sqrt{\ln\left(\frac{40\ \text{GeV}}{m_X}\right)}. \quad (38)$$

As in the nucleon case, a lower bound on the DM-electron scattering cross section can be derived by assuming that the hidden and visible sectors are in thermal equilibrium. Analogously to Eq. (34), we find

$$\sigma_e \gtrsim 3 \times 10^{-51}\ \text{cm}^2 \times \left(\frac{m_X}{10\ \text{MeV}}\right)^4 \left(\frac{10\ \text{MeV}}{m_\phi}\right)^6 \times \left(\frac{\mu_e}{0.5\ \text{MeV}}\right)^2 \sqrt{\ln\left(\frac{40\ \text{GeV}}{m_X}\right)}, \quad (39)$$

where we take $\sqrt{g_{\text{eff}}} \approx 3$.

Again, it is possible that the DM sector thermal bath evolves independently from the SM sector, and in this case, we only require the mediator to decay before BBN. From Sec. IV B, we take the bound $g_e \gtrsim 5 \times 10^{-11} \sqrt{10\ \text{MeV}/m_\phi}$. The minimum scattering cross section is

$$\sigma_e \gtrsim 3 \times 10^{-53}\ \text{cm}^2 \left(\frac{m_X}{10\ \text{MeV}}\right) \left(\frac{10\ \text{MeV}}{m_\phi}\right)^5 \times \left(\frac{\mu_e}{0.5\ \text{MeV}}\right)^2 \sqrt{\ln\left(\frac{40\ \text{GeV}}{m_X}\right)}. \quad (40)$$

If the annihilation goes through a heavier mediator $m_\phi \gg m_X$, we derive the strongest lower bound on the scattering cross section by applying CMB and relic density constraints:

$$\sigma_e \gtrsim 4 \times 10^{-39}\ \text{cm}^2 \left(\frac{10\ \text{MeV}}{m_X}\right)^2 \times \left(\frac{\mu_e}{0.5\ \text{MeV}}\right)^2 \ln\left(\frac{40\ \text{GeV}}{m_X}\right). \quad (41)$$

For electron scattering, there are no direct experimental bounds on σ_e. However, for $m_\phi < m_X$, there are bounds on σ_e arising from indirect constraints, namely, halo-shape bounds and from searches for new light gauge bosons [65]. The halo-shape constraint requires that the self-scattering cross section satisfy $\sigma_T/m_X < 4.4 \times 10^{-27}\ \text{cm}^2/\text{GeV}$ with $\sigma_T \simeq 4\pi\alpha_X^2 m_X^2/m_\phi^4$. If $m_\phi < m_X$, then constraints on new light gauge bosons rule out parts of the (m_ϕ, g_e) parameter space; we show beam-dump, supernova cooling, and electron anomalous magnetic moment constraints[10] in Fig. 5 (left panel). Here, we make use of the convention in Ref. [65], where $g_e = \epsilon e$, with the kinetic mixing parameter $\epsilon \equiv \epsilon_Y \cos\theta_W$ and e electric charge. The solid line (and shaded region) indicates the constraint.

As a simple application of the constraints discussed above, we derive the upper bound on the cross section by rewriting σ_e:

$$\sigma_e = \frac{4\mu_e^2}{\sqrt{4\pi m_X}} \sqrt{\frac{\sigma_T}{m_X}} \left(\frac{g_e}{m_\phi}\right)^2 \lesssim 3.5 \times 10^{-35}\ \text{cm}^2 \left(\frac{\mu_e}{0.5\ \text{MeV}}\right)^2 \sqrt{\frac{10\ \text{MeV}}{m_X}}. \quad (42)$$

Here, we have applied the halo-shape constraint and taken $(g_e/m_\phi)^2 \lesssim 10^{-1}\ e^2/\text{GeV}^2$, arising from measurements of the electron anomalous magnetic moment [74].

To explain more complicated constraints on the (m_X, σ_e) plane from the supernova cooling and beam-dump experiments for $m_\phi < m_X$, we show again the allowed parameter space for electron scattering cross sections, but highlight boundaries of the constraints by labeling "A", "B", and "C" in the right panel of Fig. 5. We can map excluded regions on the (m_ϕ, g_e) plane to these constraints:

(i) *Constraint A:*
For $m_\phi < m_X \lesssim 8$ MeV, supernova plus beam-dump constraints require $g_e \lesssim 1.3 \times 10^{-9}$. This places a stringent upper bound on the cross section, which we derive by taking m_ϕ to its minimum value of $m_\phi = 2m_e \approx 1$ MeV and then setting α_X to the maximum value allowed by halo-shape constraints: $\alpha_X < 9.5 \times 10^{-6} \sqrt{10\ \text{MeV}/m_X}$. This upper bound is then

$$\sigma_e \lesssim 6 \times 10^{-45}\ \text{cm}^2 \left(\frac{\mu_e}{0.5\ \text{MeV}}\right)^2 \sqrt{\frac{10\ \text{MeV}}{m_X}}. \quad (43)$$

Note that the constraint changes somewhat if we also consider $m_\phi < 1$ MeV. In this case, supernova cooling constraints still require $g_e \lesssim 1.3 \times 10^{-9}$, but halo shapes allow for a somewhat smaller m_ϕ. As a result, the upper bound is slightly weaker if we allow $m_\phi < 1$ MeV: $\sigma_e \lesssim 6 \times 10^{-44}\ \text{cm}^2 (\mu_e/0.5\ \text{MeV})^2 (10\ \text{MeV}/m_X)^{-2}$.

(ii) *Constraint B:*
This constraint applies for the large width case. In contrast with constraint A, taking $(m_\phi, g_e) = (1\ \text{MeV}, 1.3 \times 10^{-9})$ is in conflict with

[10] In general, there are also constraints from low-energy e^+e^- colliders, fixed target experiments, and neutrino experiments [13]. We find these do not significantly affect our results. In the case of kinetic mixing, bounds from measurements of the muon anomalous magnetic moment also apply. We do not include them in this paper.

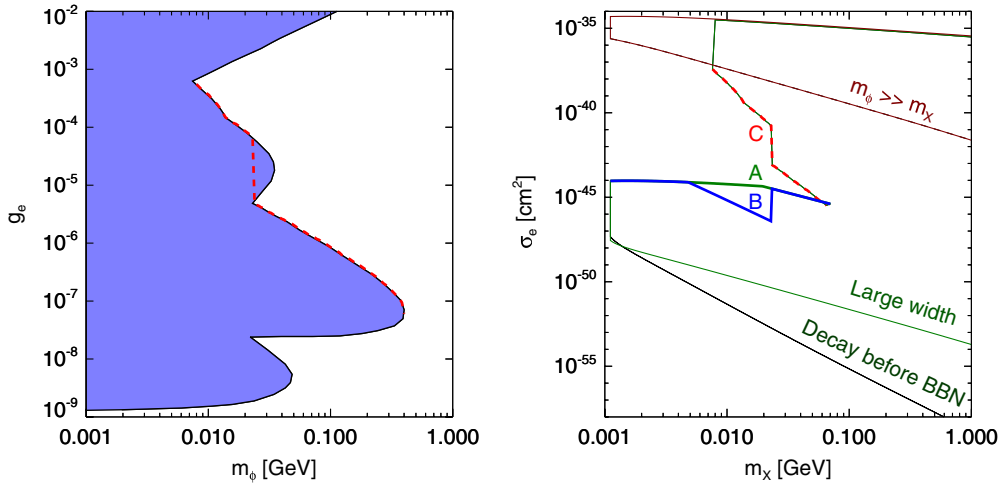

FIG. 5 (color online). *(Left)* Constraints on mediator mass m_ϕ and coupling to electrons g_e for $m_\phi < m_X$. The shaded region is excluded from electron anomalous magnetic moment, beam-dump experiments, and supernova cooling [65]. The red dashed line shows the g_e value used to derive the corresponding red dashed line (C) in the right plot. *(Right)* Constraints on electron scattering from Fig. 4. The boundaries A, B, and C are discussed in more detail in the text.

the condition of thermal equilibrium between the two sectors if the DM mass $m_X \gtrsim 5$ MeV. Furthermore, for $m_X \gtrsim 20$ MeV, the region ($m_\phi \sim 20$ MeV, $g_e \sim 3 \times 10^{-8}$) opens up. These competing effects lead to the kink in line B.

(iii) *Constraint C:*
For $m_X \gtrsim 8$ MeV, then supernova and beam-dump constraints allow a region of larger g_e: for example, ($m_\phi \sim 8$ MeV, $g_e \sim 6 \times 10^{-4}$) is now allowed. The red dashed *lower bound* on g_e in the left panel of Fig. 5 then gives rise to the constraint C. The lower bound on the cross section here comes from setting $m_\phi \sim m_X$, applying the red dashed lower bound on g_e, and setting α_X to its minimum value from CMB constraints.

We make two final notes. First, in the heavy mediator case, the beam-dump constraints do not apply, and the CMB constraints are, in general, much stronger. As a result, the high-σ_e, low-m_X region which is excluded in the light mediator case is again allowed indicated by the light red shaded region labeled $m_\phi \sim m_X$ in Fig. 4. Second, if we remove the constraint $m_\phi > 1$ MeV, ϕ will decay invisibly, and only the supernova constraints are relevant. Then, a small region of parameter space with $g_e \sim 1.3 \times 10^{-9}$ and

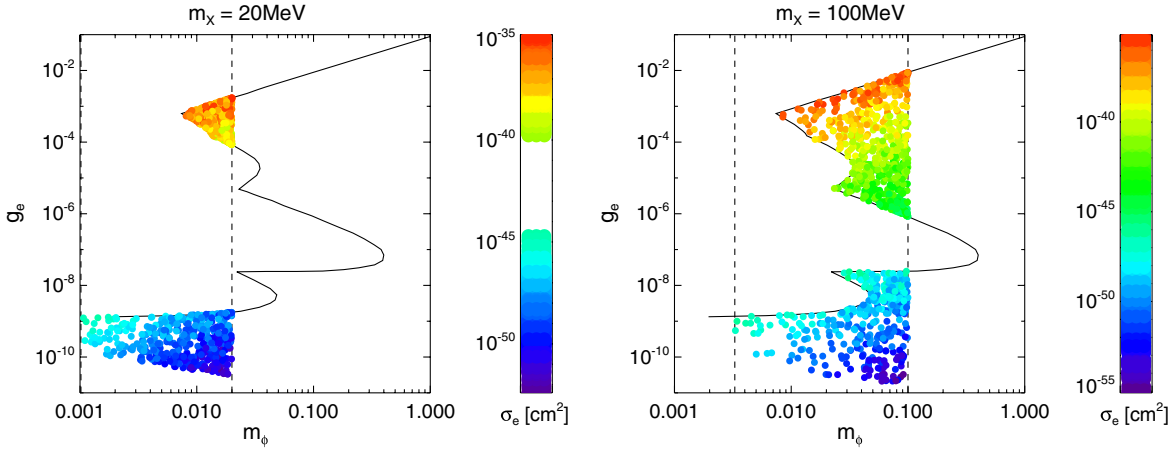

FIG. 6 (color online). For fixed m_X and a mediator with mass $m_\phi < m_X$, we generate random values of (m_ϕ, g_e) allowed by beam-dump, supernova, a_e, and BBN constraints. We show a sample of allowed points in the (m_ϕ, g_e) parameter space; the solid curve is extrapolated from the constraints in Ref. [65], also shown in the left panel of Fig. 5. For each (m_ϕ, g_e) point, we then sample the allowed α_X satisfying halo-shape and relic-density constraints and compute the corresponding elastic scattering cross section σ_e. The *color* of the point is determined by σ_e. *(Left)* $m_X = 20$ MeV, where the minimum mediator mass is $m_\phi = 1$ MeV. *(Right)* $m_X = 100$ MeV, where the minimum mediator mass $m_\phi \gtrsim 3$ MeV is set by halo-shape constraints.

$m_\phi < 1$ MeV opens up, as discussed above under constraint A.

We have verified the bounds discussed above by performing a general scan of the hidden sector parameter space. Figure 6 illustrates our method. We begin by mapping out the parameter space of (m_ϕ, g_e) and require either large ϕ width or ϕ decay before BBN. We combine this with the constraints in Ref. [65], given by the solid curve in the top panels of Fig. 6. In doing so, we impose the limit $1\ \text{MeV} < m_\phi < m_X$ for the case of $m_\phi < m_X$ and $m_\phi > 2m_X$ in the case where $m_\phi \gg m_X$. The lower limit of $m_\phi > 1$ MeV is imposed in order to allow for ϕ decay to electrons. If the halo-shape constraint gives a stronger lower bound on m_ϕ, then we take $(m_\phi)_{\text{min,halo}} < m_\phi < m_X$ for the $m_\phi < m_X$ case, where $(m_\phi)_{\text{min,halo}}$ is minimum mediator mass allowed by the halo-shape constraint. This generates the sampled points in (m_ϕ, g_e) that we have shown. For a fixed (m_ϕ, g_e), a range of values for α_X is allowed, giving rise to a range of allowed scattering cross sections. We sample random α_X values, subject to the halo-shape constraint and the relic density constraint as in Eq. (38). This then gives a randomly sampled σ_e value, which we indicate by the color of the point in Fig. 6. For a fixed m_X value, because of the range of allowed m_ϕ and α_X values, excluded regions in g_e do *not* directly map to an excluded region in σ_e. An excluded region in σ_e only arises if a sufficiently large region of g_e is excluded, as shown in the left plot of Fig. 6. We thus verify the possible values of σ_e in this way, imposing all the constraints self-consistently.

VII. CONCLUSIONS

Given the unknown nature of DM, it is important to carry out broad-based studies of models of DM. In this paper, we have examined constraints on thermal DM with mass $1\ \text{MeV} \lesssim m_X \lesssim 10$ GeV, a mass range interesting for numerous phenomenological and theoretical reasons. We considered bounds from cosmology, colliders, and astrophysics and derived implications of these constraints on direct detection.

CMB constraints on DM annihilation present the most serious challenge for light thermal DM, excluding symmetric thermal relic DM with s-wave annihilation if $m_X \lesssim 1$–10 GeV. Two natural ways to evade this constraint are to have a DM-number asymmetry or velocity-suppressed annihilation. In the asymmetric case, we found the constraint on the annihilation cross section such that the symmetric component efficiently annihilates away; the minimum cross section is larger than the usual thermal relic cross section by a factor of a few, depending on the mass.

Achieving this minimum cross section is difficult if annihilation occurs through a weak-scale (or heavier) mediator. Collider and direct-detection constraints have forced the presence of relatively light mediator states in the hidden sector in order to achieve the correct relic abundance and evade the CMB bounds. On the other hand, we found that the DM halo shape bounds on DM self-interactions require that the mediator is not too light. We examined constraints from elliptical galaxy NGC720 and elliptical clusters and derived a lower bound on the mass of the mediator particle.

We also calculated the range of scattering cross sections allowed within this scenario. Although the lowest bound which is cosmologically consistent is well below the reach of any current or envisioned direct-detection experiments, we showed that several cosmologically interesting benchmarks could be reached. For example, in the case of scattering off nucleons, a hidden sector in thermal contact with the SM at $T \sim m_X$ can be ruled out if an experiment can reach cross sections with $\sigma_n \lesssim 10^{-48}\ \text{cm}^2$. In the case of scattering off electrons, the scenario where $m_\phi \gg m_X$ can be probed by direct detection. Beam-dump and supernova constraints carve out a significant fraction of the available parameter space if $m_\phi < m_X$.

ACKNOWLEDGMENTS

We thank Doug Finkbeiner, Manoj Kaplinghat, Lisa Randall, Brian Shuve, Tracy Slatyer, Luca Vecchi, and Tomer Volansky for useful discussions. H. B. Y. and T. L. thank the Theory Division of CERN, and H. B. Y. and K. M. Z. thank the Aspen Center for Physics where part of the work was done. The work of T. L. was partially supported by NASA Theory Program Grant No. NNX10AD85G. The work of H. B. Y. and K. M. Z. was supported by NASA Theory Program Grant No. NNX11AI17G and by NSF CAREER award PHY 1049896.

[1] G. Bertone, D. Hooper, and J. Silk, Phys. Rep. **405**, 279 (2005).
[2] G. Jungman, M. Kamionkowski, and K. Griest, Phys. Rep. **267**, 195 (1996).
[3] J. L. Feng, Annu. Rev. Astron. Astrophys. **48**, 495 (2010).
[4] R. Bernabei *et al.*, Eur. Phys. J. C **67**, 39 (2010).
[5] C. Aalseth *et al.* (CoGeNT collaboration), Phys. Rev. Lett. **106**, 131301 (2011).
[6] C. E. Aalseth *et al.*, Phys. Rev. Lett. **107**, 141301 (2011).
[7] G. Angloher *et al.*, arXiv:1109.0702.

[8] C. Boehm, P. Fayet, and J. Silk, Phys. Rev. D **69**, 101302 (2004).
[9] N. Borodatchenkova, D. Choudhury, and M. Drees, Phys. Rev. Lett. **96**, 141802 (2006).
[10] D. Hooper, M. Kaplinghat, L. E. Strigari, and K. M. Zurek, Phys. Rev. D **76**, 103515 (2007).
[11] J.-H. Huh, J. E. Kim, J.-C. Park, and S. C. Park, Phys. Rev. D **77**, 123503 (2008).
[12] D. Hooper and K. M. Zurek, Phys. Rev. D **77**, 087302 (2008).
[13] P. deNiverville, M. Pospelov, and A. Ritz, Phys. Rev. D **84**, 075020 (2011).
[14] M. Pospelov, A. Ritz, and M. B. Voloshin, Phys. Lett. B **662**, 53 (2008).
[15] J. L. Feng and J. Kumar, Phys. Rev. Lett. **101**, 231301 (2008).
[16] J. L. Feng, H. Tu, and H.-B. Yu, J. Cosmol. Astropart. Phys. 10 (2008) 043.
[17] S. Nussinov, Phys. Lett. **165B**, 55 (1985).
[18] D. B. Kaplan, Phys. Rev. Lett. **68**, 741 (1992).
[19] S. M. Barr, R. S. Chivukula, and E. Farhi, Phys. Lett. B **241**, 387 (1990).
[20] D. E. Kaplan, M. A. Luty, and K. M. Zurek, Phys. Rev. D **79**, 115016 (2009).
[21] A. Falkowski, J. T. Ruderman, and T. Volansky, J. High Energy Phys. 05 (2011) 106.
[22] S. Galli, F. Iocco, G. Bertone, and A. Melchiorri, Phys. Rev. D **84**, 027302 (2011).
[23] G. Hutsi, J. Chluba, A. Hektor, and M. Raidal Astron. Astrophys. **535**, A26 (2011).
[24] D. P. Finkbeiner, S. Galli, T. Lin, and T. R. Slatyer Phys. Rev. D **85**, 043522 (2012).
[25] J. Goodman, M. Ibe, A. Rajaraman, W. Shepherd, T. M. Tait *et al.*, Phys. Lett. B **695**, 185 (2011).
[26] J. Goodman, M. Ibe, A. Rajaraman, W. Shepherd, T. M. Tait *et al.*, Phys. Rev. D **82**, 116010 (2010).
[27] Y. Bai, P. J. Fox, and R. Harnik, J. High Energy Phys. 12, (2010) 048.
[28] A. Rajaraman, W. Shepherd, T. M. Tait, and A. M. Wijangco, Phys. Rev. D **84**, 095013 (2011).
[29] P. J. Fox, R. Harnik, J. Kopp, and Y. Tsai, arXiv:1109.4398.
[30] P. J. Fox, R. Harnik, J. Kopp, and Y. Tsai, Phys. Rev. D **84**, 014028 (2011).
[31] D. Larson *et al.*, Astrophys. J. Suppl. Ser. **192**, 16 (2011).
[32] R. J. Scherrer and M. S. Turner, Phys. Rev. D **33**, 1585 (1986).
[33] T. Lin, H.-B. Yu, and K. M. Zurek (unpublished).
[34] P. Gondolo and G. Gelmini, Nucl. Phys. **B360**, 145 (1991).
[35] T. Cohen and K. M. Zurek, Phys. Rev. Lett. **104**, 101301 (2010).
[36] M. Cirelli, P. Panci, G. Servant, and G. Zaharijas, arXiv:1110.3809.
[37] M. R. Buckley and S. Profumo, Phys. Rev. Lett. **108**, 011301 (2012).
[38] M. L. Graesser, I. M. Shoemaker, and L. Vecchi, J. High Energy Phys. 10 (2011) 110.
[39] H. Iminniyaz, M. Drees, and X. Chen, J. Cosmol. Astropart. Phys. 07 (2011) 003.
[40] N. Padmanabhan and D. P. Finkbeiner, Phys. Rev. D **72**, 023508 (2005).
[41] T. R. Slatyer, N. Padmanabhan, and D. P. Finkbeiner, Phys. Rev. D **80**, 043526 (2009).
[42] S. Galli, F. Iocco, G. Bertone, and A. Melchiorri, Phys. Rev. D **80**, 023505 (2009).
[43] E. Aprile *et al.* (XENON100 Collaboration) [Phys. Rev. Lett. (to be published)], arXiv:1104.2549.
[44] M. L. Graesser, I. M. Shoemaker, and L. Vecchi, arXiv:1107.2666.
[45] J. L. Feng, M. Kaplinghat, and H.-B. Yu, Phys. Rev. D **82**, 083525 (2010).
[46] M. Kawasaki, K. Kohri, and T. Moroi, Phys. Rev. D **71**, 083502 (2005).
[47] M. Kawasaki, K. Kohri, and T. Moroi, Phys. Lett. B **625**, 7 (2005).
[48] K. Jedamzik, Phys. Rev. D **74**, 103509 (2006).
[49] M. Markevitch *et al.*, Astrophys. J. **606**, 819 (2004).
[50] J. Miralda-Escude [Astrophys. J. (to be published)], arXiv: astro-ph/0002050.
[51] J. L. Feng, M. Kaplinghat, H. Tu, and H.-B. Yu, J. Cosmol. Astropart. Phys. 07 (2009) 004.
[52] J. L. Feng, M. Kaplinghat, and H.-B. Yu, Phys. Rev. Lett. **104**, 151301 (2010).
[53] S. D. McDermott, H.-B. Yu, and K. M. Zurek, Phys. Rev. D **83**, 063509 (2011).
[54] L. Ackerman, M. R. Buckley, S. M. Carroll, and M. Kamionkowski, Phys. Rev. D **79**, 023519 (2009).
[55] J. L. Feng, V. Rentala, and Z. Surujon, Phys. Rev. D **84**, 095033 (2011).
[56] D. A. Buote, T. E. Jeltema, C. R. Canizares, and G. P. Garmire, Astrophys. J. **577**, 183 (2002).
[57] P. J. Humphrey, D. A. Buote, F. Gastaldello, L. Zappacosta, J. S. Bullock *et al.*, Astrophys. J. **646**, 899 (2006).
[58] N. Yoshida, V. Springel, S. D. White, and G. Tormen, Astrophys. J. **544**, L87 (2000).
[59] S. W. Randall, M. Markevitch,, D. Clowe, A. H. Gonzalez, and M. Bradac, Astrophys. J. **679**, 1173 (2008).
[60] M. R. Buckley and P. J. Fox, Phys. Rev. D **81**, 083522 (2010).
[61] S. A. Khrapak, A. V. Ivlev, G. E. Morfill, and S. K. Zhdanov, Phys. Rev. Lett. **90**, 225002 (2003).
[62] M. Ibe and H.-B. Yu, Phys. Lett. B **692**, 70 (2010).
[63] A. Loeb and N. Weiner, Phys. Rev. Lett. **106**, 171302 (2011).
[64] R. Essig, J. Mardon, and T. Volansky, arXiv:1108.5383.
[65] J. D. Bjorken, R. Essig, P. Schuster, and N. Toro, Phys. Rev. D **80**, 075018 (2009).
[66] G. Angloher *et al.*, Astropart. Phys. **18**, 43 (2002).
[67] J. Angle *et al.* (XENON10 Collaboration), Phys. Rev. Lett. **107**, 051301 (2011).
[68] N. Fornengo, P. Panci, and M. Regis, Phys. Rev. D **84**, 115002 (2011).
[69] M. Farina, D. Pappadopulo, A. Strumia, and T. Volansky, J. Cosmol. Astropart. Phys. 11 (2011) 010.
[70] B. Feldstein, A. Fitzpatrick, and E. Katz, J. Cosmol. Astropart. Phys. 01 (2010) 020.
[71] L. E. Strigari, New J. Phys. **11**, 105011 (2009).
[72] J. Monroe and P. Fisher, Phys. Rev. D **76**, 033007 (2007).
[73] D. Z. Freedman, Phys. Rev. D **9**, 1389 (1974).
[74] M. Pospelov, Phys. Rev. D **80**, 095002 (2009).